energies

MDPI

Article

Research on Torque Estimation Methods for Permanent Magnet Synchronous Motors Considering Dynamic Inductance Variations

Mingzhan Chen [1,*], Jie Zhang [1] and Jie Hong [2]

[1] School of Electrical and Electronic Engineering, Hubei University of Technology, Wuhan 430070, China; 19951045@hbut.edu.cn
[2] Hezhi Digital Energy Technology Co., Ltd., Wuhan 430070, China; hongjie@hicitech.com
* Correspondence: 102310345@hbut.edu.cn; Tel.: +86-181-0202-0127

Abstract

Precise electromagnetic torque estimation for permanent magnet synchronous motors (PMSMs) is crucial for enhancing the dynamic performance and energy efficiency of electric vehicles. To address the dynamic variations in dq-axis inductance caused by magnetic cross-coupling and saturation effects during motor operation—which lead to significant torque estimation errors in traditional fixed-parameter models under variable torque and speed conditions—this paper proposes a dynamic torque estimation method that integrates online dq-axis inductance identification based on a variable-step adaptive linear neural network (ADALINE) with an extended flux observer. The online identified inductance values are embedded into the extended flux observer in real time, forming a closed-loop torque estimation system with adaptive parameter updating. Experimental results demonstrate that, under complex operating conditions with varying torque and speed, the proposed method maintains electromagnetic torque estimation errors within ±3%, with a convergence time of less than 20 ms, while achieving inductance identification accuracy also within ±3%. These results significantly outperform conventional methods that do not incorporate inductance identification. This study provides a highly adaptive and engineering-practical solution for high-precision torque control of interior permanent magnet synchronous motors (IPMSMs) in automotive applications.

Keywords: extended flux observer; inductance identification; neural network; permanent magnet synchronous motor; torque estimation

Check for updates

Academic Editor: Adolfo Dannier

Received: 11 December 2025
Revised: 3 January 2026
Accepted: 8 January 2026
Published: 10 January 2026

Copyright: © 2026 by the authors. Licensee MDPI, Basel, Switzerland. This article is an open access article distributed under the terms and conditions of the Creative Commons Attribution (CC BY) license.

1. Introduction

Permanent Magnet Synchronous Motors (PMSMs) are widely applied in various fields, including electric vehicle propulsion systems, industrial precision servo control systems, and wind power generation, due to their high efficiency and excellent power density. Electromagnetic torque, as a core control parameter of the motor, directly determines the system's dynamic response performance and energy utilization efficiency. The key to electromagnetic torque estimation lies in the accurate estimation of stator flux linkage. In addressing the limitations of traditional flux observation methods, Shi WeiGuo et al. [1] proposed a novel flux observer based on a voltage–current hybrid model, which effectively combines the advantages of the voltage integration method and the current model. This approach mitigates the issue of pure integration drift to some extent, providing a more stable solution for stator flux estimation.

He Jing et al. [2] designed a discrete sliding-mode stator flux observer that accounts for resistance and inductance parameter mismatches, further enhancing the system's parameter robustness. Even under conditions where motor parameters do not match actual operating conditions, this method maintains stable performance while effectively suppressing stator flux fluctuations and electromagnetic torque ripple. Xu Anfei et al. [3] proposed an improved flux observation model that resolves observation errors through the design of a phase compensation transfer function and utilizes an extended state observer for feedforward compensation of parameter mismatch disturbances. To meet the specific requirements of sensorless control for Interior Permanent Magnet Synchronous Motors (IPMSMs), Wu Xinbing et al. [4] designed a sensorless control strategy based on a nonlinear flux observer, tailored to the structural characteristics and control needs of IPMSMs. By constructing a nonlinear observer to estimate motor flux in real time, this strategy effectively overcomes the limitations of traditional linear models under parameter mismatch and varying operating points. It provides a dedicated solution for high-performance control of these motors under sensorless conditions, further expanding the application scope of flux observation technology in complex operating scenarios.

During the actual operation of PMSMs, especially under high-load or strong excitation conditions, magnetic saturation occurs in the motor core material. This phenomenon causes the d-axis and q-axis inductances to no longer remain constant but instead become nonlinear parameters that vary significantly with the magnitude and direction of the current. Accurately describing and identifying this time-varying inductance characteristic in real time has become a key challenge in improving torque estimation and control accuracy. Chen Geng et al. [5] focused on the impact of magnetic saturation on motor parameters and proposed an online parameter identification method for these motors that accounts for magnetic saturation effects. By tracking the nonlinear variations in dq-axis inductance in real time, this method significantly enhances the accuracy of the motor model under different load conditions, providing critical insights for parameter adaptive correction in high-precision control. Xi Jianguo et al. [6] further systematically studied the online parameter identification of PMSMs, with a focus on analyzing the variation patterns of inductance parameters under dynamic operating conditions. The work provides a comprehensive analytical framework for understanding the time-varying characteristics of inductance and their impact on system performance, further emphasizing the necessity of online identification technology in addressing the nonlinear variations in motor parameters.

In the field of PMSM parameter identification, various innovative methods have been proposed. Wang Xiangsong et al. [7] constructed a Generalized Proportional–Integral Observer (GPIO) based on the motor's steady-state equations, achieving simultaneous identification of q-axis inductance and permanent magnet flux linkage. Bei Chengrong et al. [8] improved the traditional least squares algorithm by introducing a dynamically adjusted variable forgetting factor mechanism, effectively overcoming data saturation issues and enhancing anti-noise interference capability. For surface-mounted PMSMs, Wang Zhaodong et al. [9] designed an adaptive affine parameter identification algorithm that employs instantaneous d-axis field-weakening current excitation to achieve decoupled identification of multiple parameters, including stator resistance, inductance, and permanent magnet flux linkage. In the context of transient parameter identification, Liu Xu et al. [10] investigated the transient voltage equations of the motor and developed a least squares inductance identification method with a forgetting factor. This approach achieves accurate identification of relevant inductance parameters and validates its effectiveness under dynamic variations in speed and torque. Wu Chun et al. [11] proposed a novel online identification strategy that enables simultaneous real-time identification of four key parameters of PMSMs (dq-axis inductance, stator resistance, and permanent magnet

flux linkage) through voltage measurement techniques. Jing Luzong et al. [12] combined variational theory with a recurrent neural network (RNN) to propose an intelligent identification method based on the least absolute deviation approach. Mei Baishan et al. [13] focused on magnetic saturation and cross-coupling effects, establishing an accurate model for IPMSMs and achieving precise identification of dq-axis inductance under unknown parameter conditions through high-frequency voltage signal injection and pure delay filter processing.

Despite considerable advancements in parameter identification and torque estimation for PMSMs, several practical engineering challenges remain unresolved.

1. The trade-off between accuracy and speed presents a significant challenge. Least squares-based methods (e.g., [8,10]) can improve identification accuracy, yet their convergence time typically exceeds 50 ms, which is insufficient to meet the real-time identification requirements of electric vehicles. Although high-frequency signal injection [13] can accommodate magnetic saturation, it introduces additional excitation signals and increases computational overhead.
2. The separation of parameter adaptation and observer design remains a critical issue. Most existing studies treat parameter identification and state observation as independent processes. For instance, the flux observers in [1–4] enhance robustness but assume constant inductance parameters. Meanwhile, identification methods in [7–13] can track parameter variations, yet they are not integrated with observers in real time, preventing the direct improvement in torque estimation accuracy.
3. The computational complexity poses a practical constraint for embedded implementation. Methods based on recurrent neural networks [12] or sophisticated observer architectures [7], though theoretically superior, exhibit high computational demands that hinder real-time execution on automotive-grade microcontrollers such as the S32K144 employed in this work.

To address the aforementioned challenges, the core contributions of this work are summarized as follows:

1. A variable-step adaptive linear neural network is proposed, which employs an exponential step-size adjustment mechanism to balance convergence speed (<20 ms) and steady-state accuracy (±3%). This approach effectively resolves the speed–accuracy trade-off inherent in conventional LMS algorithms.
2. A closed-loop estimation system with parameter adaptation is constructed, where the real-time identified inductance parameters are fed back to the extended flux observer. This achieves deep integration between identification and observation, thereby overcoming torque estimation deviations caused by parameter mismatch.
3. The proposed method maintains high accuracy (torque error ±3%, inductance error ±3%) while exhibiting moderate computational complexity. Its feasibility has been validated on an actual automotive-grade controller, offering a practical engineering solution for high-performance electric drive systems.

2. Mathematical Model of the Permanent Magnet Synchronous Motor

Coordinate System Description

To establish the PMSM mathematical model and facilitate controller design, this paper employs two commonly used coordinate systems: the two-phase stationary coordinate system ($\alpha\beta$-frame, also known as the Clarke frame) and the two-phase rotating coordinate system (dq-frame, also referred to as the Park frame).

$\alpha\beta$-frame (Clarke frame): Through the Clarke transformation, electrical quantities in the three-phase stationary coordinate system (ABC) are converted into the two-phase

stationary coordinate system. This transformation eliminates coupling among the three-phase variables and converts time-varying three-phase sinusoidal quantities into two-phase orthogonal alternating quantities, though their amplitudes remain time-varying. The primary advantage of the $\alpha\beta$-frame lies in its stationary nature, which facilitates direct measurement and processing of stator-fixed physical quantities. It is commonly employed for instantaneous analysis of voltages and currents, as well as in the design of certain observers.

dq-frame (Park frame): Building upon the $\alpha\beta$-frame, the Park transformation rotates the two-phase stationary coordinate system into a rotating frame synchronized with the rotor. In this coordinate system, stator currents, voltages, and other AC quantities appear as DC values under steady-state operating conditions. This transformation substantially simplifies the formulation of the motor's dynamic equations and enables decoupled control of torque and flux, forming the theoretical foundation of modern motor vector control.

The transformation between the two coordinate systems is defined by the Clarke and Park transformations. Let the rotor electrical angle be denoted as θ. Then, the following relations hold:

Park transformation ($\alpha\beta \rightarrow dq$):

$$\begin{bmatrix} x_d \\ x_q \end{bmatrix} = \begin{bmatrix} cos\theta_e & sin\theta_e \\ -sin\theta_e & cos\theta_e \end{bmatrix} \begin{bmatrix} x_\alpha \\ x_\beta \end{bmatrix} \tag{1}$$

Clark transformation ($dq \rightarrow \alpha\beta$):

$$\begin{bmatrix} x_\alpha \\ x_\beta \end{bmatrix} = \begin{bmatrix} cos\theta_e & -sin\theta_e \\ sin\theta_e & cos\theta_e \end{bmatrix} \begin{bmatrix} x_d \\ x_q \end{bmatrix} \tag{2}$$

where x can represent voltage, current, or flux linkage.

Application in the proposed method: The torque estimation algorithm in this work integrates online parameter identification based on the dq-frame with extended flux observation in the $\alpha\beta$-frame. Specifically:

1. Flux observation and torque calculation (Section 3): The construction of the extended flux observer is primarily based on the motor equations in the stationary $\alpha\beta$-frame (Equation (9)). This choice is motivated by the fact that the definition of the extended flux linkages $\psi_{\alpha 1}$, $\psi_{\beta 1}$ (Equation (10)) and the observer model (Equation (18)) exhibit a more concise form in the stationary frame. This formulation avoids the complexity introduced by speed-dependent cross-coupling terms inherent in rotating coordinates, thereby simplifying the observer design and enhancing numerical stability. Finally, the electromagnetic torque is computed from the flux linkages and currents in the $\alpha\beta$-frame (Equation (12)).

2. Parameter identification stage (Section 4): The motor voltage equations are formulated in the rotating dq-frame (Equation (6)), based on which a variable-step ADALINE is designed for online identification of L_d and L_q. The dq-frame is chosen because its equation structure directly and explicitly expresses the relationship between the inductance parameters to be identified and the measurable quantities (voltages, currents, and speed). Moreover, under steady-state conditions the variables become DC quantities, which simplifies signal processing.

Through this hybrid coordinate-frame strategy—conducting parameter identification in the dq-frame and state observation in the $\alpha\beta$-frame—the proposed method fully exploits the respective advantages of each coordinate system, jointly achieving high-precision dynamic torque estimation.

The PMSM exhibits significant nonlinear characteristics and strong electromagnetic coupling between the stator and rotor during operation, making the accuracy of its math-

ematical model crucial for control performance. During motor operation, the currents injected into the three-phase stator windings—phase A, phase B, and phase C—can be expressed as follows:

$$\begin{cases} i_A = \sqrt{2}Icos(\omega_e t + \varphi) \\ i_B = \sqrt{2}Icos(\omega_e t + \varphi - 120^\circ) \\ i_C = \sqrt{2}Icos(\omega_e t + \varphi + 120^\circ) \end{cases} \tag{3}$$

where I represents the amplitude of the phase current, ω_e denotes the electrical angular velocity of the motor stator current, and φ is the initial phase angle of the phase A current.

In the two-phase rotating reference frame (dq-frame), the voltage equations of the PMSM can be expressed as:

$$\begin{cases} u_d = R_s i_d + \frac{d\psi_d}{dt} - \omega_e \psi_q \\ u_q = R_s i_q + \frac{d\psi_q}{dt} - \omega_e \psi_d \end{cases} \tag{4}$$

where ψ_d and ψ_q are the dq-axis components of the stator flux linkage, and i_d and i_q are the dq-axis components of the stator current. R_s denotes the stator resistance.

The flux linkage equations can be expressed as:

$$\begin{cases} \psi_d = L_d i_d + \psi_f \\ \psi_q = L_q i_q \end{cases} \tag{5}$$

where L_d and L_q represent the inductances of the stator winding along the direct-axis (d-axis) and quadrature-axis (q-axis), respectively, and ψ_f denotes the flux linkage produced by the rotor permanent magnets.

Substituting Equation (3) into Equation (2) yields the relationship between the dq-axis voltages and the dq-axis currents:

$$\begin{cases} u_d = R_s i_d + L_d \frac{di_d}{dt} - \omega L_q i_q \\ u_q = R_s i_q + L_q \frac{di_q}{dt} + \omega \left(L_d i_d + \psi_f \right) \end{cases} \tag{6}$$

At this point, the electromagnetic torque equation in the two-phase rotating reference frame can be written as:

$$T_e = \frac{3}{2} p_n \left[\psi_f i_q + (L_d - L_q) i_d i_q \right] \tag{7}$$

where p_n is the number of pole pairs of the motor.

In the stationary $\alpha\beta$ reference frame, the mathematical expression for electromagnetic torque can be derived as:

$$T_e = \frac{3}{2} p_n (\psi_\alpha i_\beta - \psi_\beta i_\alpha) \tag{8}$$

where ψ_α and ψ_β are the αβ-axis components of the stator flux linkage, and i_α and i_β are the $\alpha\beta$-axis components of the stator current.

3. Extended Flux Linkage Principle and Observer Construction

3.1. Principle of Extended Flux Linkage

Considering the rapid current response, Equation (4) can be expressed in the two-phase stationary reference frame as:

$$\begin{bmatrix} u_\alpha \\ u_\beta \end{bmatrix} = \begin{bmatrix} R_s + DL_q & 0 \\ 0 & R_s + DL_q \end{bmatrix} \begin{bmatrix} i_\alpha \\ i_\beta \end{bmatrix} + D \left\{ \left[(L_d - L_q) i_d + \psi_f \right] \begin{bmatrix} cos\theta \\ sin\theta \end{bmatrix} \right\} \tag{9}$$

where u_α and u_β are the $\alpha\beta$-axis components of the stator voltage, and θ is the rotor electrical angle, $D = \frac{d}{dt}$.

The second term on the right-hand side of Equation (7) corresponds to the differential term of the extended flux linkage, which can be expressed in the two-phase stationary reference frame as:

$$\begin{bmatrix} \psi_{\alpha 1} \\ \psi_{\beta 1} \end{bmatrix} = \left[(L_d - L_q) i_d + \psi_f \right] \begin{bmatrix} cos\theta \\ sin\theta \end{bmatrix} \tag{10}$$

where $\psi_{\alpha 1}$ and $\psi_{\beta 1}$ are the $\alpha\beta$-axis components of the stator extended flux linkage.

Based on the mathematical model of the PMSM, the relationship between the stator flux linkage and the extended flux linkage of the motor can be expressed by the following equation:

$$\begin{bmatrix} \psi_\alpha \\ \psi_\beta \end{bmatrix} = L_q \begin{bmatrix} i_\alpha \\ i_\beta \end{bmatrix} + \begin{bmatrix} \psi_{\alpha 1} \\ \psi_{\beta 1} \end{bmatrix} \tag{11}$$

Based on the extended flux linkage, the electromagnetic torque expression for the PMSM can be established as:

$$T_e = \frac{3}{2} p_n \left(L_q \begin{bmatrix} i_\alpha & i_\beta \end{bmatrix} + \begin{bmatrix} \psi_{\alpha 1} & \psi_{\beta 1} \end{bmatrix} \right) J \begin{bmatrix} i_\alpha \\ i_\beta \end{bmatrix} \tag{12}$$

where J is the coefficient matrix:

$$J = \begin{bmatrix} 0 & -1 \\ 1 & 0 \end{bmatrix} \tag{13}$$

3.2. State Observer Construction

To design an extended flux linkage observer, it is necessary to first establish the state-space model of the PMSM. Based on the principle of extended flux linkage (Equation (10)) and its dynamic characteristics, the state equation for the extended flux linkage can be expressed as:

$$D\psi_{\alpha\beta 1} = \omega_e J \psi_{\alpha\beta 1} \tag{14}$$

where $\psi_{\alpha\beta 1}$ is the state variable, given by:

$$\psi_{\alpha\beta 1} = \begin{bmatrix} \psi_{\alpha 1} \\ \psi_{\beta 1} \end{bmatrix} \tag{15}$$

The standard form of the system equation for the state observer is:

$$\begin{cases} \frac{dx}{dt} = Ax + Bu \\ y = Cx \end{cases} \tag{16}$$

According to Equation (14), the coefficient matrices are defined as follows:

$$\begin{cases} A = \omega_e J = \begin{bmatrix} 0 & -\omega_e \\ \omega_e & 0 \end{bmatrix} \\ B = \begin{bmatrix} 0 & 0 \\ 0 & 0 \end{bmatrix} \\ C = \omega_e J = \begin{bmatrix} 0 & -\omega_e \\ \omega_e & 0 \end{bmatrix} \end{cases} \tag{17}$$

Based on the above derivations, the complete dynamic equation of the extended flux linkage observer can be established as:

$$\begin{bmatrix} \psi_{\alpha 1} \\ \psi_{\beta 1} \end{bmatrix} = \int \begin{bmatrix} -\omega k_2 \psi_{\alpha 1} \\ \omega k_3 \psi_{\beta 1} \end{bmatrix} + \int \begin{bmatrix} u_\alpha - R_s i_\alpha + k_2 (u_\beta - R_s i_\beta) - L_q \frac{di_\alpha}{dt} + k_2 \frac{di_\beta}{dt} \\ u_\beta - R_s i_\beta + k_3 (u_\alpha - R_s i_\alpha) - L_q \frac{di_\beta}{dt} + k_3 \frac{di_\alpha}{dt} \end{bmatrix} \tag{18}$$

where k_2 and k_3 are the feedback coefficients. According to the stability criterion, the extended flux linkage observer converges when $k_2 > 0$ and $k_3 < 0$.

4. *dq*-Axis Inductance Identification Method

4.1. Analysis of the Variable-Step Adaptive Linear Neural Network Algorithm

To achieve online identification of dq-axis inductances, this paper adopts an ADALINE as the core identification unit. ADALINE is a classical single-layer linear neural network originally proposed by Widrow and Hoff, which updates its network weights online using the least mean square (LMS) algorithm. It features a simple structure and low computational load, making it suitable for real-time parameter identification in embedded systems. Its fundamental structure, shown in Figure 1, consists of an input layer, a weight layer, and an output layer, where the weight vector $W(k)$ corresponds to the inductance parameters to be identified. In contrast to conventional ADALINE, a variable step-size mechanism is introduced in this work, allowing the network to adaptively adjust its learning rate.

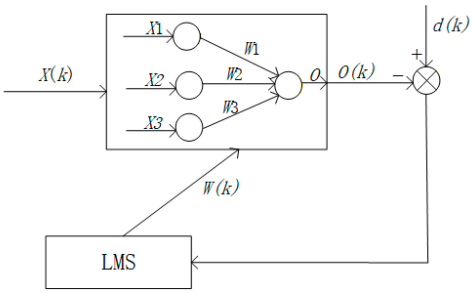


Figure 1. Basic Structure of the Adaptive Linear Neural Network.

In Figure 1, the variables $X(k)$, $O(k)$, $W(k)$, and $d(k)$ represent the input, output, weight, and desired output of the network at time kT_s, respectively. The adaptive update of the network weights is implemented using the Least Mean Square (LMS) algorithm, with its specific computational procedure described as follows:

$$\begin{cases} W(k+1) = W(k) + 2\eta(k)X(k)\varepsilon(k) \\ \varepsilon(k) = d(k) - W(k)X(k) \\ O(k) = W(k)X(k) \end{cases} \tag{19}$$

where $\eta(k)$ denotes the step-size factor for weight updating, and $\varepsilon(k)$ represents the error signal between the network output and the desired output. To ensure convergence of the LMS algorithm, the step size $\eta(k)$ must satisfy the following constraint:

$$0 < 2\eta(k)|X(k)|^2 < 1 \tag{20}$$

The variable-step mechanism designed in this paper establishes a functional relationship between the step size and the square of the error at the current time instant. This design offers dual advantages: the step size automatically decreases as the system approaches

steady state, and it depends solely on the current error without being influenced by past error sequences. The specific algorithm formulation is as follows:

$$\eta(k) = \beta\left(1 - \frac{1}{1 + \alpha|\varepsilon(k)|^2}\right) \tag{21}$$

where $\alpha > 0$ is the shape factor, controlling how the step size varies with the error. A larger α accelerates the transition of the step size from its minimum to its maximum value. $\beta > 0$ is the maximum step-size limit, defining the upper bound of the step size, i.e., $\lim_{|\varepsilon(k)|\to\infty} \eta(k) = \beta$. In this paper, α = 2 and α = 0.08.

4.2. Variable-Step Adaptive Linear Neural Network for Inductance Identification

To formulate a neural-network-identifiable structure, Equation (4) is reformulated into a linear parameterized equation model:

$$\begin{bmatrix} u_d - R_s i_d \\ u_q - R_s i_q - \omega_e \psi_f \end{bmatrix} = \begin{bmatrix} \frac{di_d}{dt} & -\omega_e i_q \\ \omega_e i_d & \frac{di_q}{dt} \end{bmatrix} \begin{bmatrix} L_d \\ L_q \end{bmatrix} \tag{22}$$

Construction of the Input Vector:

$$X(k) = \begin{bmatrix} x_1(k) \\ x_2(k) \\ x_3(k) \\ x_4(k) \end{bmatrix} = \begin{bmatrix} \frac{di_d}{dt}(k) \\ -\omega_e(k) i_q(k) \\ \omega_e(k) i_d(k) \\ \frac{di_q}{dt}(k) \end{bmatrix} \tag{23}$$

Construction of the Output Vector:

$$O(k) = \begin{bmatrix} O_d(k) \\ O_q(k) \end{bmatrix} = \begin{bmatrix} L_d(k)\frac{di_d}{dt}(k) - \omega_e(k) L_q(k) i_q(k) \\ \omega_e(k) L_d(k) i_d(k) + L_q(k)\frac{di_q}{dt}(k) \end{bmatrix} \tag{24}$$

The error between the output vector $O(k)$ and the desired output vector $d(k)$, defined as $\varepsilon(k) = d(k) - O(k)$, is used to drive the weight update. This process, combined with the variable-step mechanism, enables rapid convergence and steady-state control.

Construction of the Desired Output Vector:

$$d(k) = \begin{bmatrix} d_1(k) \\ d_2(k) \end{bmatrix} = \begin{bmatrix} u_d(k) - R_s i_d(k) \\ u_q(k) - R_s i_q(k) - \omega_e(k)\psi_f \end{bmatrix} \tag{25}$$

where the voltages u_d and u_q, currents i_d and i_q, and electrical angular velocity ω_e are measured in real time, while the stator resistance R_s and permanent magnet flux linkage ψ_f are known constants.

Construction of the Weight Vector (i.e., Identification Vector):

$$W(k) = \begin{bmatrix} w_1(k) \\ w_2(k) \end{bmatrix} = \begin{bmatrix} L_d(k) \\ L_q(k) \end{bmatrix} \tag{26}$$

The adaptive law of the variable-step adaptive linear neural network is developed based on stochastic gradient descent. By formulating the inductance identification problem as an instantaneous squared error minimization problem, the gradient direction for weight updating is derived. To address the conflict between convergence speed and steady-state accuracy inherent in the traditional LMS algorithm with a fixed step size, an exponential

variable-step function is introduced. This allows the learning rate to adaptively adjust according to the magnitude of the current error.

Definition of the Instantaneous Squared Error Cost Function:

$$J(k) = \frac{1}{2}||\varepsilon(k)||^2 = \frac{1}{2}[d(k) - U(k)W(k)]^T[d(k) - U(k)W(k)] \tag{27}$$

where $U(k) = \begin{bmatrix} \frac{di_d}{dt}(k) & -\omega_e(k)i_q(k) \\ \omega_e(k)i_d(k) & \frac{di_q}{dt}(k) \end{bmatrix}$.

Applying the stochastic gradient descent method, the weights are updated along the negative gradient direction of the cost function:

$$W(k+1) = W(k) - \eta(k)\nabla_W J(k) \tag{28}$$

Calculation of the Gradient:

$$\nabla_W J(k) = -U(k)^T \varepsilon(k) \tag{29}$$

Substituting this yields the adaptive law:

$$W(k+1) = W(k) + \eta(k)U(k)^T \varepsilon(k) \tag{30}$$

4.3. Extended Robustness Analysis

4.3.1. Purpose and Scope of the Analysis

The core contribution of this chapter lies in achieving real-time identification of the dynamically varying direct- and quadrature-axis inductances (L_d and L_q). Theoretically, however, the overall performance of torque estimation could also be influenced by mismatches in other motor parameters. Among these, the stator resistance *Rs*—which varies significantly in practice due to winding temperature rise—constitutes a potential factor worthy of attention. To comprehensively evaluate the engineering practicality of the proposed method, this subsection employs simulation analysis to focus on examining the robustness of the closed-loop system—integrating the "variable-step ADALINE online identification + extended flux observer"—to variations in the R_s parameter. It should be clarified that the content of this section constitutes an extended analysis based on a simulation model, aiming to explore the robustness boundaries of the method at a theoretical level; the subsequent Section 6 will validate its actual performance using a physical experimental platform.

4.3.2. Simulation Model and Testing Conditions

To maintain consistency in the analysis, the simulation was conducted within the MATLAB/Simulink environment. The parameters of the established PMSM model are identical to those of the experimental motor described in Section 6, and the same control architecture is employed (SVPWM-based vector control with a switching frequency of 5 kHz). To test the robustness under the most demanding conditions, the simulation scenario adopts the high-speed step-load operating condition from Section 5: the target speed is 1800 RPM, and the load torque steps from 0 to 70 N·m at t = 2.0 s.

To emulate the gradual variation in the stator resistance caused by temperature rise, the actual R_s value in the simulation motor model is increased stepwise from its nominal value (0.02 Ω) to predetermined higher values (+20%, +30%, +40%) after the load transient has settled and the system reaches a steady state (t = 2.5 s). Meanwhile, the R_s parameter used in the proposed ADALINE identifier module remains fixed at the original nominal value (0.02 Ω). This setup simulates a practical scenario where a permanent parame-

ter mismatch occurs due to the lack of temperature monitoring or compensation in the actual system.

4.3.3. Results and Analysis of Stator Resistance Variation Effects

The simulation results of key performance metrics under different R_s variation levels are presented in Table 1. For comparison, the performance of the conventional fixed-parameter observer (without online parameter identification) under the same R_s variations is also listed.

Table 1. Simulation Assessment of Stator Resistance Variation Effects on System Performance.

R_s Variation Scenario	Actual R_s Value (Ω)	Steady-State Torque Estimation Error (%)	Convergence Time After R_s Step (ms)	L_d Identification Steady-State Error (%)	L_q Identification Steady-State Error (%)
Nominal case (Baseline)	0.020	±2.5	–	±2.7	±2.9
+20% variation	0.024	±3.6	<22	±3.3	±3.5
+30% variation	0.026	±4.3	<23	±3.6	±3.8
+40% variation	0.028	±4.9	<25	±3.9	±4.1
Conventional fixed-parameter method (+30% variation)	0.026	±9.7	>35	–	–

According to the results presented in Table 1, it can be observed that:

1. Controllable Performance Degradation: When the actual R_s increases by +30%, the steady-state torque estimation error of the proposed method rises from the baseline ±2.5% to ±4.3%, an increase of approximately 1.8 percentage points. Even under a substantial +40% variation, the error remains strictly bounded within ±5%.
2. Robust Dynamic Response: Following a step change in R_s, the system's torque estimate reconverges to the new steady state within 25 ms, demonstrating the closed-loop system's excellent dynamic adaptive capability.
3. Maintained Significant Advantage: Under the same +30% R_s variation, the torque estimation error of the proposed method (±4.3%) is less than half of that of the conventional fixed-parameter method (±9.7%), highlighting the core benefit of integrating online parameter identification.

4.3.4. Results Analysis and Engineering Implications

The above simulation results indicate that the proposed torque estimation method integrating online inductance identification exhibits good inherent robustness to moderate variations in the stator resistance R_s. This primarily stems from two reasons: First, as can be seen from the motor torque equation (Equation (7)), the sensitivity of electromagnetic torque to the inductance parameters Ld and L_q is generally much higher than its sensitivity to the stator resistance R_s, especially in the medium- to high-load region. Second, the employed variable-step ADALINE possesses adaptive learning capability; its weight adjustment mechanism can, to some extent, absorb the equivalent disturbance generated by R_s mismatch, thereby mitigating its overall impact on the final output accuracy.

Engineering Application Significance: For most industrial applications and electric vehicle powertrain systems, a torque estimation accuracy within ±5% is sufficient to meet the requirements of high-performance control. Therefore, even if R_s undergoes certain variations due to temperature rise during actual operation, the proposed method can still provide reliable and usable torque observations, demonstrating direct engineering practicality.

4.4. System Implementation Architecture

Figure 1 details the internal structure of the variable-step ADALINE, which serves as the core identification unit within the overall control system. To clearly demonstrate the engineering implementation of the aforementioned theoretical methods, Figure 2 presents the overall block diagram of the IPMSM control system integrated with online inductance identification. The correspondence between the modules in the diagram and the preceding theoretical sections is as follows:

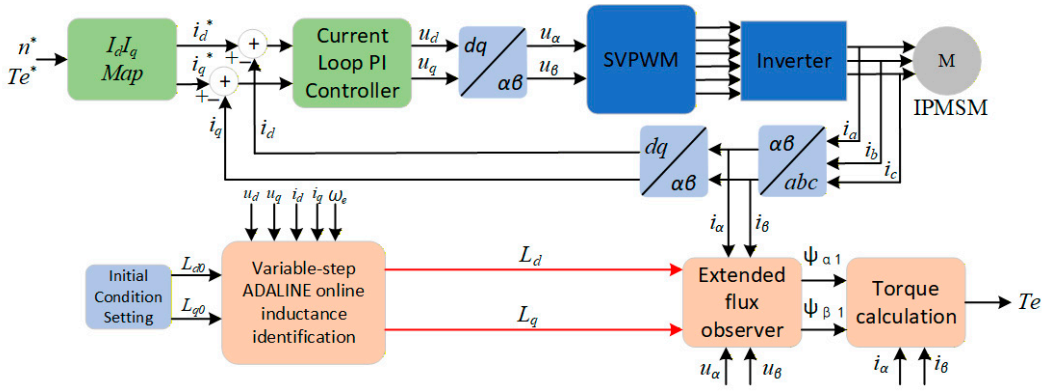


Figure 2. Control Block Diagram of the IPMSM System. Symbols with an asterisk (e.g., n^*, T_e^*, i_d^*, i_q^*) denote given values (n^*: given speed; T_e^*: given torque; i_d^*,: given d-axis current; i_q^*: given q-axis current).

1. dq-axis current and voltage sampling and coordinate transformation module: This module acquires the three-phase motor currents and voltages, which are then transformed via Clarke and Park transformations to obtain i_d, i_q, u_d, and u_q. These signals serve as inputs for subsequent modules.
2. Variable-step ADALINE online inductance identification module: Corresponding to Sections 4.1 and 4.2, this module implements the identification algorithm specified by Equations (19)–(30). It takes i_d, i_q, u_d, u_q, and the electrical angular velocity ω_e as inputs, and outputs the identified inductances L_d and L_q in real time. Its internal network structure is detailed in Figure 1. Its internal computational flow strictly follows the theoretical derivation:
   (1). The input vector $X(k)$ is constructed according to Equation (23);
   (2). The desired output vector $d(k)$ is calculated based on Equation (25);
   (3). The weight update is performed via the variable-step LMS algorithm of Equation (30), with the step size $\eta(k)$ adaptively adjusted by Equation (21);
   (4). The weight vector $W(k)=\begin{bmatrix} L_d(k) \\ L_q(k) \end{bmatrix}$ constitutes the identification result.
3. Extended flux observer module: Corresponding to Section 3.2, this module calculates the flux linkage according to Equation (18). The key innovation lies in its real-time reception of the inductance parameters L_d and L_q from the ADALINE module, enabling dynamic updates of its internal model instead of relying on fixed parameters.
4. Torque calculation module: Based on Equation (12), this module computes the electromagnetic torque Te using the observed flux linkages $\psi_{\alpha 1}$, $\psi_{\beta 1}$ and the currents i_α, i_β.
5. Real-time parameter feedback path (red arrow in the figure): This path indicates that the identified parameters L_d and L_q are fed back to the observer at every control cycle, forming a closed-loop estimation system with parameter adaptation.

5. Computational Complexity Analysis and Experimental Implementation Considerations

5.1. Computational Complexity of the Variable-Step ADALINE

To assess the feasibility of the proposed algorithm on resource-constrained automotive-grade microcontrollers, this section performs a quantitative analysis of its computational complexity. The main operations executed within each control cycle (T_s = 0.2 ms, corresponding to a 5 kHz switching frequency) can be broken down as follows:

Forward computation (Equation (19)): Calculation of the network output $O(k) = W(k)X(k)$, which involves the multiplication of a 2×4 weight matrix by a 4×1 input vector, requiring a total of 8 multiplications and 6 additions.

Error computation: Calculation of $\varepsilon(k) = d(k) - W(k)X(k)$, requiring 2 subtraction operations.

Variable-step update (Equation (21)): Computation of the adaptive learning rate $\eta(k) = \beta\left(1 - \frac{1}{1+\alpha|\varepsilon(k)|^2}\right)$, which includes the squared error norm (2 multiplications and 1 addition), scalar multiplication, addition, and one division, totaling approximately 8–10 operations. The division operation is relatively time-consuming in embedded systems.

Weight update (Equation (30)): Execution of $W(k+1) = W(k) + \eta(k)U(k)^T \varepsilon(k)$, involving matrix operations and scalar multiplication, requiring approximately 32 multiply–accumulate operations.

In addition, overheads such as data access, loop control, and function calls must be taken into account. Based on a comprehensive estimation, the core portion of the algorithm requires approximately 70–85 equivalent floating-point operations per control cycle.

5.2. Experimental Implementation and Real-Time Verification

The algorithm was implemented on an experimental platform based on the NXP S32K144 microcontroller (ARM Cortex-M4F core, 80 MHz clock frequency, with single-precision floating-point unit, FPU). To accurately evaluate its execution time, the GPIO toggle method was employed for measurement: a GPIO pin is set high at the entry of the ADALINE update function and cleared low at its exit, and an oscilloscope is used to capture the pulse width.

Repeated test results show that executing one complete ADALINE parameter update takes an average of 12.5 μs (with a standard deviation of approximately 1.2 μs). This duration accounts for only 6.25% of the 200 μs control period, leaving ample computational margin for other critical tasks in the system.

6. Test Verification

6.1. Experimental Setup and Instrumentation

To ensure the reproducibility and credibility of the experimental results, this subsection provides a detailed description of the key components and of the test platform.

6.1.1. Core Controller and Drive System

Microcontroller Unit (MCU): The proposed algorithm was implemented on an NXP S32K144 automotive-grade MCU (NXP Semiconductors, Eindhoven, The Netherlands) (ARM Cortex-M4F (ARM Limited, Cambridge, UK), 80 MHz, with FPU). The control period (Ts) was set to 200 μs, corresponding to a 5 kHz PWM switching frequency.

Power Drive Module: A three-phase voltage source inverter (VSI) based on 650V/100A IGBTs (Infineon Technologies AG, Neubiberg, Germany) (Infineon FS100R07N3E4) was used. The gate drivers featured reinforced isolation and desaturation protection.

Sensor and Sampling:

Current Sensing: Two galvanically isolated Hall-effect current sensors (LEM LAH 100-P, LEM International SA, Geneva, Switzerland) were used for two-phase current measurement. The signals were sampled by the MCU's 12-bit ADC at 5 kHz.

Voltage Sensing: DC bus voltage and three-phase PWM terminal voltages were measured via isolated voltage sensors (LEM LV 100 (LEM International SA, Geneva, Switzerland)) and resistive dividers.

Position/Speed Feedback: A 17-bit absolute encoder (Tamagawa TS5700N840 (Tamagawa Seiki Co., Ltd., Matsumoto, Japan)) was mounted on the motor shaft to provide accurate rotor position and speed information.

6.1.2. Reference Measurement Benchmarks

Actual Torque Measurement: The motor under test was mechanically coupled to a Magtrol HD-715-8BN (Magtrol, Inc., Buffalo, NY, USA) hysteresis dynamometer via a torque flange. A high-precision, non-contact torque sensor (HBM T22 (Hottinger Brüel & Kjær, Darmstadt, Germany), 0–100 N·m range, accuracy class 0.05) was installed inline between the motor and the dynamometer to provide the ground-truth torque value (T_e_actual). Its output was recorded by a separate data acquisition system (NI PXIe-1073 (National Instruments Corporation, Austin, TX, USA)) at 10 kHz.

Actual Inductance Calibration: The "actual" dq-axis inductance values (L_d_actual, L_q_actual), used as the reference for online identification error calculation, were obtained through a rigorous offline calibration procedure:

Standstill Frequency Response Test: The motor was held at a fixed rotor position (d-axis and q-axis aligned, respectively). A series of low-amplitude, variable-frequency sinusoidal voltage signals (10 Hz to 1 kHz) were injected into the relevant axis. The impedance was measured using a precision impedance analyzer (Keysight E4990A (Keysight Technologies, Santa Rosa, CA, USA)).

Finite Element Analysis (FEA) Correction: To account for the difference between small-signal and large-signal operation, a 2D FEA model of the IPMSM was built in ANSYS Maxwell (Version 2023 R1). The model was tuned to match the measured frequency response data at low flux levels.

Load-Dependent Mapping: The calibrated FEA model was then used to simulate the motor's magnetic characteristics under various id and iq current combinations, generating lookup tables of L_d_actual(i_d, i_q) and L_q_actual(i_d, i_q). These tables served as the benchmark during dynamic experiments.

6.1.3. Load and Control System

Dynamometer System: The Magtrol dynamometer, controlled by a DSP-6001 controller (Magtrol, Inc., Buffalo, NY, USA), operated in torque mode to apply the precise load profiles (ramp and step) specified in the experiments.

Host Computer and Software: A PC running MATLAB/Simulink (Version R2023a) was connected to the MCU via CAN bus. It was used for parameter configuration, real-time data monitoring, and triggering the predefined load sequences from the dynamometer controller.

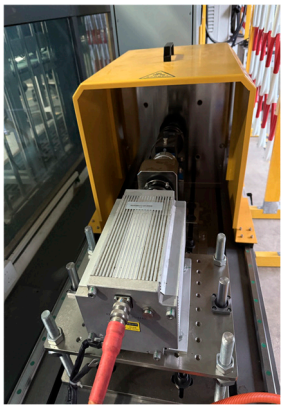
6.2. Experimental Procedure and Validation

Based on the aforementioned test platform, the effectiveness of the proposed method was validated. An IPMSM experimental platform, as shown in Figure 3, was constructed. The platform is centered around an NXP S32K144 microcontroller (NXP Semiconductors N.V., Eindhoven, The Netherlands), integrated with a power drive module, current and voltage sampling circuits, and an encoder interface circuit, forming a complete motor vector control system. The specific parameters of the experimental motor are listed in Table 2,

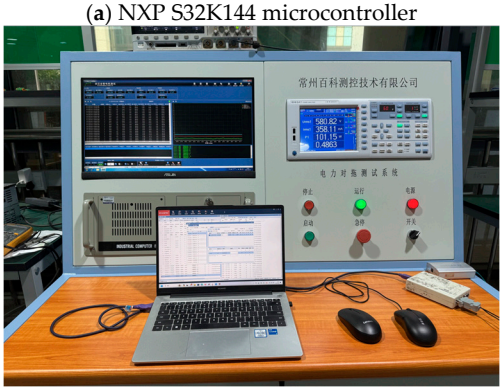
with the system switching frequency set to 5 kHz. The actual torque values were measured using a high-precision torque sensor, while the actual inductance values were calibrated offline via frequency response analysis combined with finite element simulation, serving as a reference benchmark for the online identification results. The load torque was applied by a matching dynamometer test bench. During the experiments, start commands were first sent from the host computer to initiate the motor under no-load conditions and stabilize it at the target speed. Once the speed stabilized, torque commands were transmitted from the measurement and control computer to the load bench to simulate varying load conditions.



(**a**) NXP S32K144 microcontroller



(**b**) Interior permanent magnet synchronous motor



(**c**) Host computer and control console



(**d**) High-voltage DC power supply

Figure 3. Key components of the IPMSM experimental platform. (**a**) NXP S32K144 automotive-grade microcontroller; (**b**) Interior permanent magnet synchronous motor (IPMSM) under test; (**c**) Host computer and motor control console; (**d**) High-voltage DC power supply unit.

Table 2. Parameters of the Motor.

Parameters	Value
DC Bus Voltage U_{dc}(V)	610
Rated TorqueTe_N(N·m)	70
Rated Speed n_N(RPM)	1800
Permanent Magnet Flux Linkage$\psi_f(W_b)$	0.1
Stator Resistance $R_s(\Omega)$	0.02
Stator d-Axis Inductance L_d(mH)	9.8
Stator q-Axis Inductance L_q(mH)	21.9
Number of Pole Pairs p_n	4

To verify the operational performance of the proposed control strategy under different speed ranges and loading conditions, experiments were conducted at selected speed values from both high- and low-speed regions. The experimental conditions were set as follows:

High-speed case: The motor target speed was set to 1800 RPM. After maintaining the target speed under no-load for 2 s, a load that ramped up uniformly to 70 N·m was applied. The motor then continued to operate under the constant load torque of 70 N·m.

High-speed step-load case: The motor target speed was 1800 RPM. After 2 s of no-load operation at the target speed, a step load of 70 N·m was abruptly applied. The motor subsequently maintained the load torque of 70 N·m.

Low-speed step-load case: The motor target speed was 300 RPM. After 2 s of no-load operation at the target speed, a step load of 30 N·m was abruptly applied. The motor then continued to run under the constant load torque of 30 N·m.

Figure 4 illustrates the dynamic speed response curve as the motor starts and undergoes a uniform load increase to 70 N·m, reaching 1800 RPM. During the no-load startup phase, the acceleration period is 0.5 s, with the speed rapidly rising to the target value. At approximately 1 s, an overshoot of about 6% occurs, demonstrating the system's favorable dynamic response characteristics. This overshoot decays quickly within 0.5 s, and the speed returns to stability. At the 2 s mark, a load torque that ramps uniformly from 0 N·m to 70 N·m is applied via the dynamometer, resulting in a speed dip of about 3%. The system recovers to the target speed again within 0.5 s, indicating that the proposed control strategy possesses strong disturbance-rejection capability and excellent speed-recovery performance.

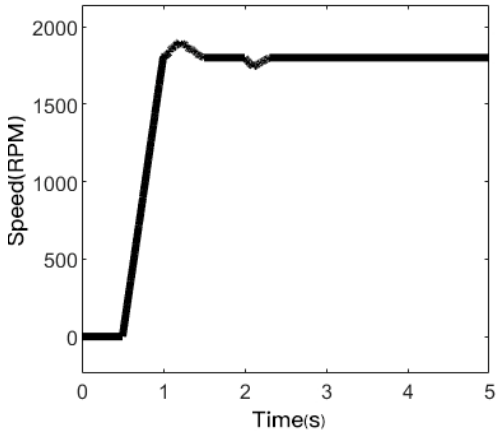


Figure 4. Speed Response at 1800 RPM under Uniform Load Ramp.

Figure 5 compares the impact of inductance identification on torque estimation. After the load torque ramps uniformly to 70 N·m, the conventional observer without inductance identification exhibits a noticeable estimation error, with a steady-state error of approximately ±7% of the actual torque. In contrast, the observer incorporating inductance identification rapidly and accurately tracks the actual torque variation, achieving a significantly improved steady-state estimation accuracy with the error confined within ±2.7%. A closer examination of the local convergence process in Figure 6 shows that after the load command changes, the estimated torque from the observer with inductance identification converges to the actual torque within about 20 ms, demonstrating fast dynamic response and minimal overshoot. By comparison, the conventional observer without parameter identification exhibits sluggish convergence, along with appreciable steady-state deviation and dynamic lag. A quantitative comparison of torque-estimation performance is provided in Table 3.

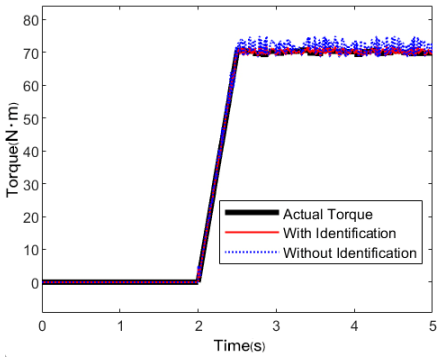


Figure 5. Comparison of Torque Estimation with and without Inductance Identification.

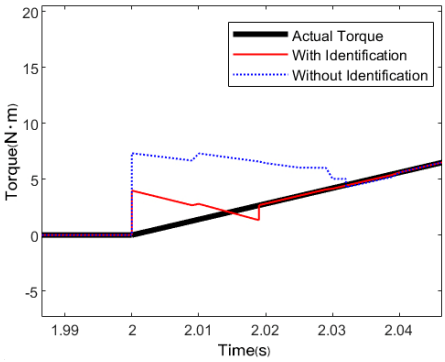


Figure 6. Comparison of Torque Convergence Processes.

Table 3. Comparison of Torque Estimation Performance at 1800 RPM with Uniform Load Ramp.

With vs. Without Inductance Identification	Steady-State Accuracy (%)	Convergence Time (ms)	Overshoot (N·m)
With	±2.7	<20	<5
Without	±7	>20	<10

Figure 7 presents the identification results of the dq-axis inductances during a linear increase in load torque from 0 N·m to 70 N·m. As the load torque gradually rises, the magnetic saturation effect inside the motor intensifies, causing the actual value of L_d to decrease from approximately 9.8 mH initially to about 6.6 mH, while the actual value of L_q drops from about 21.9 mH to around 16.4 mH, exhibiting a characteristic nonlinear attenuation. The proposed identification algorithm effectively tracks this variation process; the estimated curves align well with the actual curves, and the identification error remains within ±2.8%, verifying the effectiveness and robustness of the online identification.

Figure 8 shows the speed waveform during motor startup and a step increase to 70 N·m, with the speed rising to 1800 RPM. In the no-load startup stage, the system responds rapidly, achieving acceleration within 0.5 s. The speed exhibits an overshoot at around 1 s, with a peak overshoot of about 6%, which quickly decays and returns to steady state within 0.5 s, indicating good dynamic tracking performance. At 2 s, a step load torque of 70 N·m is applied to the motor, causing a speed dip with a maximum drop of approximately 8%. The system recovers to the given speed within 1 s, demonstrating strong disturbance-rejection and recovery capability. The experimental results confirm that the proposed control method maintains satisfactory speed stability and dynamic regulation quality even under high-speed step-load conditions.

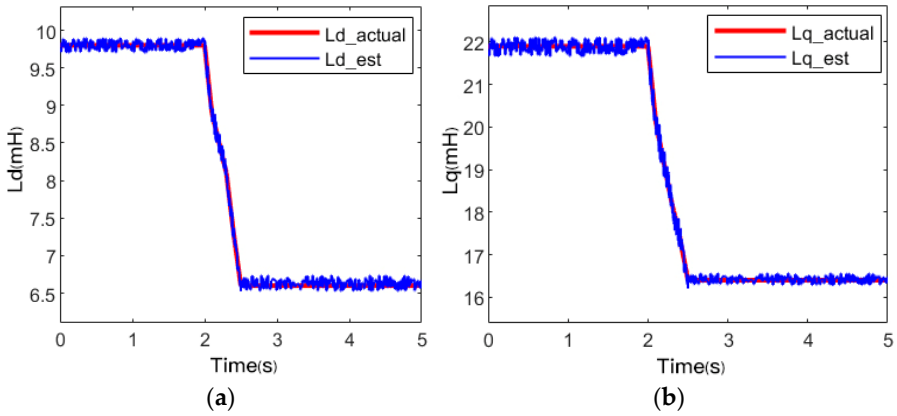


Figure 7. (**a**) Identification Results of the *d*-Axis Inductance. (**b**) Identification Results of the *q*-Axis Inductance.

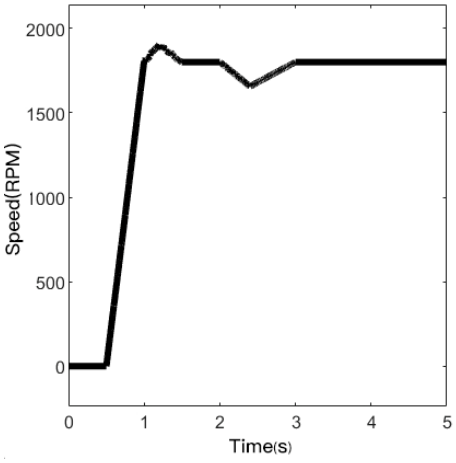


Figure 8. Speed Response at 1800 RPM under Step Load Change.

Figure 9 compares the impact of inductance identification on torque-estimation performance under high-speed step-load conditions. After the load torque steps to 70 N·m, the observer without inductance identification shows noticeable dynamic lag and steady-state deviation, with a steady-state estimation error reaching ±10% of the actual torque. In contrast, the observer incorporating online inductance identification tracks the torque variation more rapidly and accurately, delivering smoother dynamic response and significantly improved steady-state estimation accuracy, with the error confined within ±2.8%. A closer look at the local convergence process of the torque step response in Figure 10 reveals that at the instant the load torque steps to 70 N·m, the estimated value from the observer with online inductance identification converges within about 20 ms with negligible overshoot. By comparison, the conventional observer without parameter identification exhibits markedly slower convergence and sustained steady-state deviation. A quantitative comparison of the torque-estimation performance is provided in Table 4.

Table 4. Comparison Table of Estimated Torque Performance at 1800 RPM with Sudden Load Increase.

With vs. Without Inductance Identification	Steady-State Accuracy (%)	Convergence Time (ms)	Overshoot (N·m)
With	±2.8	<20	<5
Without	±10	>20	<10

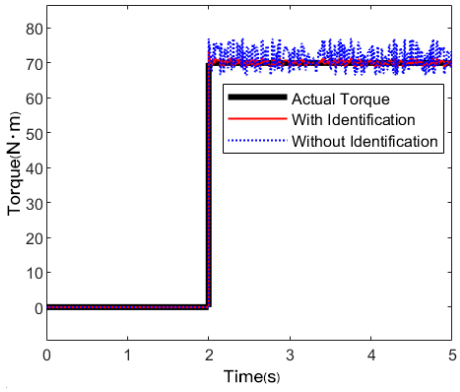


Figure 9. Comparison of Torque Estimation with and without Inductance Identification.

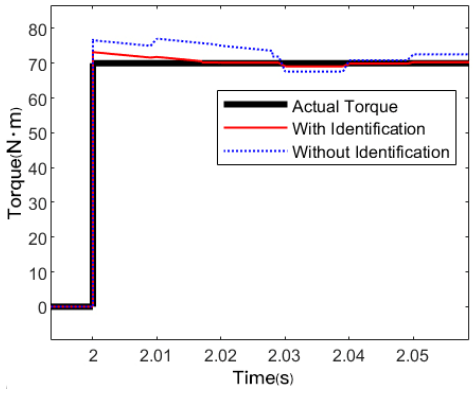
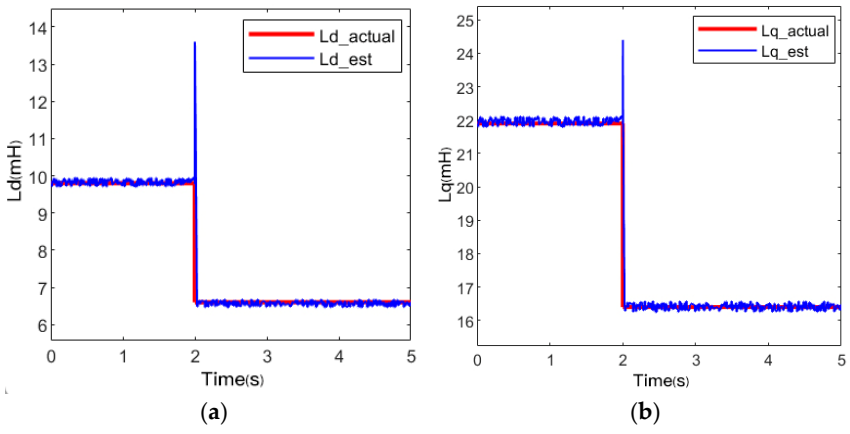


Figure 10. Comparison of Torque Convergence Processes.

Figure 11a presents the online identification results of the *d*-axis inductance when the load torque steps to 70 N·m. It can be observed that at the instant of the step load change, the q-axis current increases sharply, causing rapid saturation of the q-axis magnetic path. Meanwhile, due to magnetic coupling and the dynamic current regulation transient, the identified value of L_d~ exhibits a brief rise—from an initial value of about 9.8 mH to a peak of approximately 13.6 mH—followed by fast convergence within 30 ms, eventually settling near a steady-state value of around 6.6 mH. The identification results closely follow the actual variation trend throughout the process, with the steady-state identification error maintained within ±2.7%.



(**a**) (**b**)

Figure 11. (**a**) Identification Results of the *d*-Axis Inductance. (**b**) Identification Results of the *q*-Axis Inductance.

Figure 11b shows the online identification results of the q-axis inductance under the same step load of 70 N·m. At the moment of the load step, the dynamic cross-saturation effect and the transient coupling of current response lead to a short-term increase in the identified L_q, which jumps from an initial value of 21.9 mH to about 23.9 mH and then converges rapidly within 24 ms, finally stabilizing near a steady-state value of approximately 16.4 mH. The steady-state identification error for the q-axis inductance remains within ±3%. These results demonstrate that the proposed online identification method possesses good dynamic tracking capability and steady-state accuracy under high-speed step-load conditions.

Figure 12 shows the speed response curve during motor startup and a step increase to 30 N·m, with the speed rising to 300 RPM. During the no-load startup phase, the acceleration time is 0.5 s, and the speed rapidly rises to the set value. An overshoot of approximately 3% occurs at about 1 s, after which the speed quickly recovers and stabilizes at the target speed, demonstrating favorable dynamic response characteristics and stability of the control system. At 2 s, a step load torque of 30 N·m is applied to the system, resulting in a speed dip of about 5%. The system exhibits effective disturbance-rejection and regulation capability, recovering to the given speed within 1 s. The experimental results indicate that even under low-speed step-load conditions, the proposed control method maintains a relatively fast speed-recovery rate and good steady-state accuracy, verifying its effectiveness and robustness in practical operation.

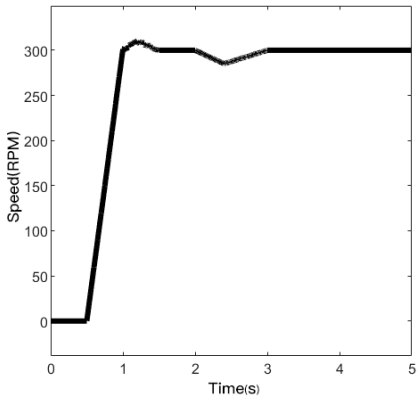


Figure 12. Speed Response at 300 RPM under Step Load Change.

Figure 13 compares the impact of inductance identification on torque-estimation performance under low-speed step-load conditions. After the load torque steps to 30 N·m, the observer without inductance identification exhibits a noticeable steady-state deviation, with its torque estimate fluctuating around the actual value and a steady-state error range of approximately ±9%. In contrast, the observer incorporating online inductance identification tracks the actual torque variation more rapidly and smoothly, delivers a more timely dynamic response, and achieves significantly improved steady-state estimation accuracy, with the error confined within ±2.5%. A closer inspection of the local convergence process of the torque step response in Figure 14 shows that at the instant the load torque steps to 30 N·m, the observer with inductance identification converges to the steady-state actual torque within about 15 ms, exhibiting fast dynamic response and negligible overshoot. On the other hand, the conventional observer without parameter identification displays markedly slower convergence, longer settling time, and sustained oscillations. A quantitative comparison of the torque-estimation performance is detailed in Table 5.

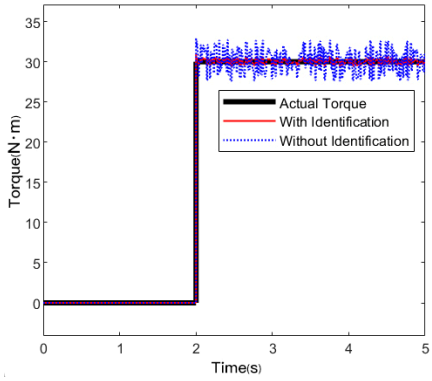


Figure 13. Comparison of Torque Estimation with and without Inductance Identification.

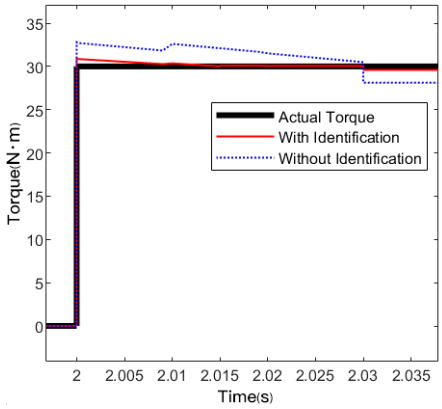


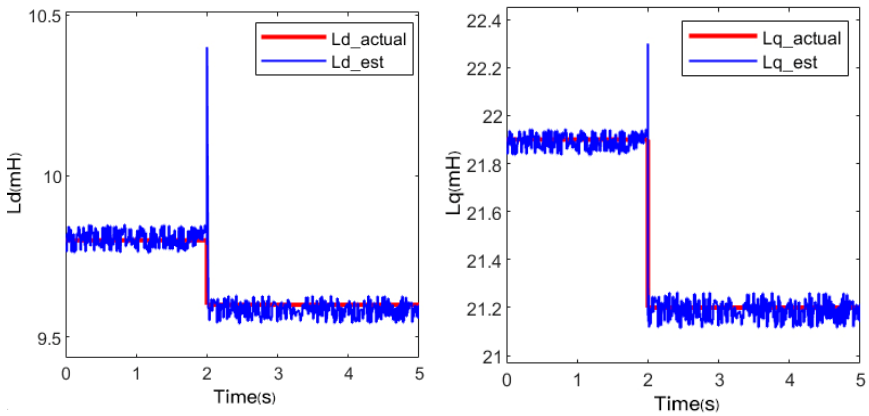
Figure 14. Comparison of Torque Convergence Processes.

Table 5. Comparison Table of Estimated Torque Performance at 300 RPM with Sudden Load Increase.

With vs. Without Inductance Identification	Steady-State Accuracy (%)	Convergence Time (ms)	Overshoot (N·m)
With	±2.5	<20	<3
Without	±9	>20	<5

Figure 15a presents the actual variation and online identification results of the d-axis inductance when the load torque steps to 30 N·m. At the instant of the step load change, magnetic-circuit coupling causes the identified value of L_d to undergo a brief rise from the initial value of 9.8 mH to about 10.4 mH. It then converges rapidly within 24 ms and finally stabilizes near a steady-state value of approximately 9.6 mH. The steady-state identification error remains within ±2.6%.

Figure 15b shows the actual variation and online identification results of the q-axis inductance under the same 30 N·m step load. Immediately after the load step, dynamic cross-saturation effects and transient coupling in the current loop lead to a short-term increase in the identified L_q, from an initial value of 21.9 mH to about 22.3 mH. The value then converges within 20 ms and settles near a steady-state value of around 21.2 mH, with the steady-state identification error kept within ±2.9%. The experiments demonstrate that the proposed online identification method effectively tracks both the dynamic characteristics and steady-state changes of L_q under low-speed step-load conditions, exhibiting good dynamic response capability and steady-state accuracy.



(**a**) (**b**)

Figure 15. (**a**) Identification Results of the *d*-Axis Inductance. (**b**) Identification Results of the *q*-Axis Inductance.

7. Discussion

7.1. Comparison and Interpretation of Results in the Context of Prior Research

This study directly addresses the core challenge of time-varying parameters in high-precision control of Permanent Magnet Synchronous Motors (PMSMs) caused by magnetic saturation and cross-coupling. As noted in Chen et al. [5] and Xi et al. [6], the dynamic variation in inductance parameters is the primary reason for the performance degradation of traditional fixed-parameter models under high-load and high-speed operating conditions. While Wang et al. [7] to Mei et al. [13] have proposed various online parameter identification strategies (e.g., Generalized Proportional–Integral Observer, variable forgetting factor least squares, high-frequency signal injection, etc.), which have improved the tracking capability for time-varying parameters to some extent, these methods often either prioritize steady-state accuracy at the expense of dynamic response speed, or involve high computational complexity, imposing stringent real-time requirements on processors.

In contrast, the variable-step ADALINE online identification mechanism proposed in this paper effectively balances the trade-off between convergence speed and steady-state accuracy by constructing an exponential variable-step function to adaptively adjust the learning rate (Equation (19)). Experimental results (Figures 7, 11 and 15) demonstrate that the proposed method achieves rapid convergence within 20–30 ms during transient processes such as load step changes and ramp loading, while maintaining the steady-state identification error of the dq-axis inductances within ±3% throughout. This performance surpasses that of the identification scheme based on the traditional least squares method in Liu et al. [10], which exhibits limitations in convergence speed and disturbance rejection under dynamic operating conditions.

At the torque estimation level, Shi et al. [1] to Wu et al. [4] focus on enhancing the robustness of stator flux estimation by improving flux observers (e.g., voltage–current hybrid models, sliding-mode observers, nonlinear observers), but most are based on the assumption of constant parameters. When the motor actually operates in the magnetic saturation region, the estimation accuracy of these methods degrades significantly. As shown in Figures 5 and 9, the steady-state error of traditional observers without inductance identification reaches as high as ±7% to ±10%. The innovation of this work lies in constructing a parameter-adaptive closed-loop estimation system: the real-time identified inductance values are fed back to the extended flux observer (Equation (16)), enabling the observer model to dynamically follow changes in the internal magnetic state of the motor. Consequently, even under a highly saturated 70 Nm load, the proposed method strictly confines the torque estimation error within ±3%, with a convergence time of less

than 20 ms (Figures 6, 10 and 14). This confirms the necessity of deeply integrating online parameter identification with high-performance observers, providing an effective pathway to overcome the performance limitations of traditional methods under varying parameter conditions.

To more clearly delineate the contributions of this study, a quantitative comparison of performance metrics is conducted from two dimensions: parameter identification and torque estimation. Representative methods from recent literature are evaluated, with Table 6 focusing on PMSM parameter identification techniques and Table 7 dedicated to torque estimation methods.

Table 6. Comparison of PMSM Parameter Identification Methods.

Method Category	Representative Literature	Inductance Identification Accuracy (%)	Convergence Time (ms)	Computational Complexity	Magnetic Saturation Adaptability	Main Limitations
Least Squares + Forgetting Factor	Bei et al. [8] and Liu et al. [10]	±5	>50	Medium	Good	Slow dynamic response
High-frequency Signal Injection	Mei et al. [13]	±4	>30	High	Excellent	High system complexity
Recurrent Neural Network Method	Jing et al. [12]	±4	>30	Very High	Excellent	Heavy computational burden
Proposed Method (ADALINE)	This work	±3	<20	Medium–Low	Excellent	Requires validation under extreme conditions

Table 7. Comparison of PMSM Torque Estimation Methods.

Method Category	Representative Literature	Torque Estimation Accuracy (%)	Convergence Time (ms)	Magnetic Saturation Adaptability
Traditional Fixed-Parameter Model	Baseline	±7–10	>30	Poor
Improved Flux Observer	Shi et al. [1] to Wu et al. [4]	±7–10	>30	Moderate
Proposed Method	This work	±3	<20	Excellent

In terms of parameter identification, existing methods generally face the trade-off dilemma among "accuracy, speed, and complexity". For instance, while Bei et al. [8] and Liu et al. [10] improve accuracy through algorithmic enhancements, their convergence time exceeds 50 ms. Although Mei et al. [13] achieves higher precision, it introduces high-frequency signals, resulting in increased system complexity and potential control interference. This paper employs a variable-step ADALINE with an adaptive learning-rate mechanism, which maintains high accuracy of ±3% while reducing convergence time to below 20 ms. Moreover, its computational complexity is rated as "medium-low", making it more suitable for embedded implementation.

In the domain of torque estimation, most existing studies still rely on fixed-parameter models or non-real-time parameter updates. Although the observers in Shi et al. [1] to Wu et al. [4] feature structural optimizations, their neglect of inductance variations leads to errors of ±7–10% in the saturation region. This work innovatively establishes a real-time parameter-state closed-loop system, where identification results are fed back to the extended flux observer within milliseconds. This enables torque estimation accuracy to reach ±3% with a convergence time of <20 ms, while maintaining stability even under deep saturation at 70 N·m.

7.2. Broader Context and Implications of the Findings

The findings of this work hold significant dual implications for both theory and engineering. At the theoretical level, it validates that integrating data-driven methods such as the adaptive linear neural network with traditional physics-based motor state observation theory can effectively address the strong nonlinearity and time-varying nature inherent in motor systems. The constructed "identification–observation" closed-loop framework offers a transferable paradigm for handling parameter uncertainties and state estimation problems in a wider range of electromechanical systems.

At the engineering application level, the value of this method is particularly pronounced in the field of new energy vehicle propulsion. The traction motors in electric vehicles frequently operate under complex conditions characterized by wide speed ranges and rapid torque variations, placing extremely high demands on the dynamic response accuracy and robustness of the control system. The proposed scheme achieves high-precision real-time torque estimation with relatively low computational complexity (based on the lightweight ADALINE), meeting the stringent requirements for real-time performance and reliability in automotive-grade controllers. Experimental results demonstrate that the method maintains superior performance across different speeds (300 RPM and 1800 RPM) and under different load variation patterns (step and ramp), proving its strong environmental adaptability and engineering practicality. This provides key technical support for the development of next-generation high-performance, high-efficiency electric drive systems.

7.3. Future Research Directions

While this study has achieved positive outcomes, it also points to several directions for future research:

1. Validation under Extreme Conditions and Lifetime Testing: The experiments were primarily conducted in a laboratory environment. Future work should involve long-term validation under more extreme real-world vehicle conditions, such as varying temperatures and vibrations, as well as throughout the entire operational lifecycle, to assess the durability and reliability of the method.
2. Embedded Algorithm Optimization: Although the current algorithm has been implemented on a microcontroller, there remains room for further optimization. For instance, investigating more concise network topologies or integrating the approach with other intelligent control algorithms could enhance its applicability on resource-constrained platforms.
3. Extension to Other Motor Types: The proposed method is designed based on the IPMSM mathematical model. Its core concept—addressing parameter variations through online identification—holds universal potential. Future research could explore extending this approach to other motor types with significant parameter variations, such as synchronous reluctance motors (SynRM) and switched reluctance motors (SRM).

8. Conclusions

This paper addresses the issue of time-varying dq-axis inductance in automotive IPMSMs caused by magnetic saturation and cross-coupling during operation. A dynamic torque estimation method is proposed, which integrates online inductance identification based on a variable-step adaptive linear neural network with an extended flux observer. The method uses the neural network to identify inductance parameters in real time and feeds them back to the extended flux observer, thereby establishing a parameter-adaptive closed-loop torque estimation system.

Experimental results demonstrate that the proposed method exhibits superior performance under different rotational speeds (300 RPM and 1800 RPM) and various load variation patterns (ramp loading and step loading):

1. Significant improvement in torque estimation accuracy: With the introduction of inductance identification, the steady-state error of torque estimation is confined within $\pm 3\%$, representing a marked improvement compared to traditional methods without inductance identification, which exhibit errors of $\pm 7\%$ to $\pm 10\%$.
2. Enhanced dynamic response speed: The convergence time of torque estimation is reduced to less than 20 ms, with minimal dynamic overshoot.
3. High accuracy in inductance identification: The identification error of the dq-axis inductances remains within $\pm 3\%$ across all operating conditions, enabling accurate tracking of the nonlinear variations induced by magnetic saturation.
4. Strong system disturbance rejection: The system demonstrates fast speed recovery and small overshoot under sudden load changes, reflecting excellent robustness.

In summary, the proposed method effectively resolves the torque estimation errors caused by time-varying inductance, achieving high-precision and fast-response dynamic electromagnetic torque estimation. It provides an engineering-practical solution for enhancing the dynamic performance and energy efficiency of automotive IPMSM control systems.

Author Contributions: Conceptualization, J.H.; methodology, M.C.; software, M.C.; validation, M.C.; formal analysis, M.C.; investigation, M.C.; resources, J.H.; data curation, M.C.; writing—original draft preparation, M.C.; writing—review and editing, J.Z.; visualization, M.C.; supervision, J.Z. and J.H.; project administration, J.Z. and J.H.; funding acquisition, none. All authors have read and agreed to the published version of the manuscript.

Funding: This research received no external funding.

Data Availability Statement: The original contributions proposed in this study are included within the manuscript. For further inquiries, please contact the corresponding author.

Conflicts of Interest: Author Jie Hong was employed by the company Hezhi Digital Energy Technology Co., Ltd. The remaining authors declare that the research was conducted in the absence of any commercial or financial relationships that could be construed as a potential conflict of interest.

References

1. Shi, W.; Sang, Y. A New Magnetic Flux Observer Based on a Voltage-Current Hybrid Model. *Electr. Mach. Control. Appl.* **2019**, *46*, 14–19.
2. He, J.; Li, Z.; Wu, G. Robust model predictive control of stator magnetic flux for permanent magnet synchronous motors based on improved multi-vector selection. *Sci. Technol. Eng.* **2025**, *25*, 610–620. [CrossRef]
3. Xu, A.; Zhu, X.; Yuan, L. A hybrid model flux observer for permanent magnet synchronous motors considering phase compensation and parameter mismatch. *J. Power Supply* **2025**, 1–15.
4. Wu, X.; Zhang, W.; Feng, S. Sensorless control of built-in permanent magnet synchronous motor based on nonlinear magnetic flux observer. *Micro Spec. Mot.* **2024**, *52*, 44–48. [CrossRef]
5. Chen, G.; Yang, S.; Zhang, X. Online parameter identification of permanent magnet synchronous motors considering magnetic saturation effects. *J. Power Supply* **2024**, 1–13.
6. Xi, J.; Feng, Y.; Zhao, B.; Gao, J. Research on Online Parameter Identification of Permanent Magnet Synchronous Motors. *J. Chongqing Univ. Technol. (Nat. Sci.)* **2023**, *37*, 289–296.
7. Wang, X.; Yang, S.; Xie, Z.; Zhang, X. Magnetic Flux Prediction Control of Permanent Magnet Synchronous Motor Based on Multi-Parameter Identification. *J. Electr. Eng. Technol.* **2024**, *39*, 7084–7098. [CrossRef]
8. Bei, C.; Lu, W.; Lu, Y.; Dong, X.; Fang, D.; Yue, B.; You, L. Identification of electrical parameters of permanent magnet synchronous motors based on the variable forgetting factor recursive least squares method. *Electron. Technol.* **2025**, *38*, 9–19. [CrossRef]
9. Wang, Z.; Hu, X.; Mei, L.; Wang, F. Online identification of permanent magnet synchronous motor parameters based on affine algorithm. *J. Power Supply* **2023**, 1–14.

10. Liu, X.; Wang, X.; Wang, S.; Liang, L.; Huang, J. Research on Inductance Identification of Permanent Magnet Synchronous Motor Based on Least Squares Method. *Electr. Mach. Control. Appl.* **2020**, *47*, 1–5+23. [CrossRef]
11. Wu, C.; Zhao, Y.; Sun, M. Online identification of multiple parameters for permanent magnet synchronous motors using voltage measurement. *China Electr. Power Eng. J.* **2020**, *40*, 4329–4340. [CrossRef]
12. Jing, L.; Wu, Q. Research on Parameter Identification of Permanent Magnet Synchronous Motor Based on Recurrent Neural Networks. *Electr. Drive* **2020**, *50*, 87–91. [CrossRef]
13. Mei, B.; Zhang, P. Identification of inductance parameters of built-in permanent magnet synchronous motor based on high-frequency signal injection. *Micro Spec. Mot.* **2019**, *47*, 52–55.

Disclaimer/Publisher's Note: The statements, opinions and data contained in all publications are solely those of the individual author(s) and contributor(s) and not of MDPI and/or the editor(s). MDPI and/or the editor(s) disclaim responsibility for any injury to people or property resulting from any ideas, methods, instructions or products referred to in the content.